Since January 2020 Elsevier has created a COVID-19 resource centre with free information in English and Mandarin on the novel coronavirus COVID-19. The COVID-19 resource centre is hosted on Elsevier Connect, the company's public news and information website.

Journal of Theoretical Biology 557 (2023) 111334

Contents lists available at ScienceDirect

Journal of Theoretical Biology

journal homepage: www.elsevier.com/locate/yjtbi

Antibody protection from SARS-CoV-2 respiratory tract exposure and infection

Alex Chen [a,*], Timothy Wessler [b], M. Gregory Forest [b,c,d]

[a] Department of Mathematics, California State University—Dominguez Hills, Carson, CA 90747, USA
[b] Department of Mathematics, University of North Carolina—Chapel Hill, Chapel Hill, NC 27599, USA
[c] Department of Applied Physical Sciences, University of North Carolina—Chapel Hill, Chapel Hill, NC 27599, USA
[d] UNC/NCSU Joint Department of Biomedical Engineering, University of North Carolina—Chapel Hill, Chapel Hill, NC 27599 and North Carolina State University, Raleigh, NC 27606, USA

ARTICLE INFO

Keywords:
SARS-CoV-2
Mechanistic modeling
Muco-trapping antibodies
Neutralizing antibodies
Mucus

ABSTRACT

The COVID-19 pandemic has underscored the need to understand the dynamics of SARS-CoV-2 respiratory infection and protection provided by the immune response. SARS-CoV-2 infections are characterized by a particularly high viral load, and further by the small number of inhaled virions sufficient to generate a high viral titer in the nasal passage a few days after exposure. SARS-CoV-2 specific antibodies (Ab), induced from vaccines, previous infection, or inhaled monoclonal Ab, have proven effective against SARS-CoV-2 infection. Our goal in this work is to model the protective mechanisms that Ab can provide and to assess the degree of protection from individual and combined mechanisms at different locations in the respiratory tract. Neutralization, in which Ab bind to virion spikes and inhibit them from binding to and infecting target cells, is one widely reported protective mechanism. A second mechanism of Ab protection is muco-trapping, in which Ab crosslink virions to domains on mucin polymers, effectively immobilizing them in the mucus layer. When muco-trapped, the continuous clearance of the mucus barrier by coordinated ciliary propulsion entrains the trapped viral load toward the esophagus to be swallowed. We model and simulate the protection provided by either and both mechanisms at different locations in the respiratory tract, parametrized by the Ab titer and binding-unbinding rates of Ab to viral spikes and mucin domains. Our results illustrate limits in the degree of protection by neutralizing Ab alone, the powerful protection afforded by muco-trapping Ab, and the potential for dual protection by muco-trapping and neutralizing Ab to arrest a SARS-CoV-2 infection. This manuscript was submitted as part of a theme issue on "Modelling COVID-19 and Preparedness for Future Pandemics".

1. Introduction

The COVID-19 pandemic has raised the urgent need for deeper scientific knowledge and understanding of respiratory infections. The immediate needs from science have evolved in parallel with the SARS-CoV-2 virus throughout the pandemic: understanding the most prevalent sources of exposure and between-host transmission of infection (Johnson and Morawska, 2009; Morawska et al., 2009; Kushalnagar et al., 2021; Yang et al., 2020); understanding within-host transmission of infection (Ke et al., 2021; Moses et al., 2021); understanding the degrees of immunity acquired from infection and vaccines; understanding the mechanisms of immune system protection. These needs from science are enormous, spanning individuals to communities at all scales, for trusted guidance on personal behavior and protection, medical treatment, and public health policy.

Many within-host models of SARS-CoV-2 infection are based on ordinary differential equations governing susceptible and infected cell populations, virus, infection and replication dynamics, and some incorporate aspects of immune response. Carruthers et al. (Carruthers et al., 2022); Goyal et al. (Goyal et al., 2021), and Ke et al. (Ke et al., 2021) modeled the conversion of an initially susceptible population of cells to states of infection and viral shedding over time, and thereby infer

Peer review under responsibility of for items with item group IG000060: VSI: Regulatory circuits add the footnote "This article is further included in a special issue of JTB dedicated to the memory of Prof. René THOMAS." the text "special issue of JTB dedicated to the memory of Prof. René THOMAS" should have the hyperlink to the VSI page: "https://www.sciencedirect.com/journal/journaloftheoreticalbiology/specialissue/100J1T9ZH1F".

* Corresponding author.
E-mail address: achen@csudh.edu (A. Chen).

https://doi.org/10.1016/j.jtbi.2022.111334
Received 1 July 2022; Received in revised form 12 October 2022; Accepted 18 October 2022
Available online 25 October 2022

key model parameters from viral titer data (Wolfel et al., 2020; Kissler et al., 2021). These works then deduced important public health metrics such as the between-host transmission time window and polymerase chain reaction (PCR) test-positivity over time. Coupled with a spatial map of susceptible cells, one can further account for spatial dynamics of infected cells and viral load. The SimCov model (Moses et al., 2021) extends the approach of (Ke et al., 2021) by explicit resolution of a spatial grid of susceptible cells, and concludes that an important factor that may influence severity of infection is the spatial separation of infection seeds, a similar conclusion reached by (Chen et al., 2022). Mucociliary clearance (MCC) is another important spatial effect, accounting for the competition between advection of the mucus layer and diffusion of species (virions and immune agents) within. A recent spatial model of influenza (Quirouette et al., 2020) incorporates the role of MCC in a 1-D model of upper respiratory tract infection. In a 3-D, agent-based spatial infection model of the nasal passage and all generations of the lower respiratory tract (LRT) (Chen et al., 2022), it was shown that *MCC plays conflicting roles when presented with a novel virus* (i.e., prior to or absent of immune response): *protection* by clearing significant percentages of infectious SARS-CoV-2 virions toward the esophagus to be swallowed into the stomach; *acceleration* of the number and spatial spread of infected cells and shed virions by strong mucus advection in the nasal passage and upper branches of the LRT; and *localization* in the presence of very weak advection in the deep lung, so that infectious seeds deposited in the deep lung remain localized and cannot be transported upward and cleared on timecales relevant for protection. Therefore, in sufficient numbers, deeper infection seeds result in severe infection.

In this paper, we explore within-host SARS-CoV-2 human respiratory infections in the presence of antibody protection. We extend the physiologically faithful, predictive modeling framework in (Chen et al., 2022) by incorporating known and hypothetical mechanisms underlying antibody (Ab) protection against human respiratory infection. The mechanisms that contribute to the degree of Ab protection to SARS-CoV-2 or any viral pathogen are diverse, including: physiology of the respiratory tract, including MCC; the percentage of infectable epithelial cells by the virus; how infectable the cells are; once infected, the kinetics of cellular assembly and replication of infectious progeny before cell death; and, with new model extensions beyond (Chen et al., 2022); *how antibodies specific to the virus or to the mucosal barrier of the respiratory tract interrupt or prevent infection.* The model presented here is calibrated to SARS-CoV-2; the framework, however, is adaptable to any respiratory virus.

Over the past 2 + years, we developed a *pre-immunity* model of within-host respiratory tract (RT) exposure and infection to the novel coronavirus SARS-CoV-2 (Chen et al., 2022). The model is an agent-based stochastic model that tracks both viruses and infected cells while encoding details noted above: the physiological landscape of each generation of the respiratory tract, including dimensions of the air core, the airway surface liquid (ASL) coating the epithelium, the epithelial surface area, and the percentage of infectable cells; upon inhaled deposition at any generation in the RT, the physical processes of viral diffusion and advection (while in the mucus layer) in the airway surface liquids of each generation; encounters with and infection probabilities of epithelial cells; and the kinetics of infected cell assembly, replication, and shedding of infectious progeny until cell death. This baseline model provides predictions of *outcomes* from inhaled exposures to SARS-CoV-2 throughout the respiratory tract except for the nasopharynx and oropharynx where the geometry and features of MCC are more complex. *Outcomes* consist first of the likelihood of clearance versus infection as a function of the respiratory tract location of deposition of an inhaled infectious seed. Next, from a successful infection and location in the respiratory tract, the model simulates the progression of viral load and infected cells in the immediate hours and days after the initial infection, again assuming the immune system is not activated on these timescales.

In this paper, we extend this baseline stochastic model of SARS-CoV-2 respiratory tract exposure and infection to include two modes of protection provided by antibodies (Ab), detailed next. The model also accommodates the timing (prior to or after onset of infection) and "dosage" (Ab concentration) of Ab protection at each generation in the upper or lower respiratory tract. *For all specified inputs, and for each generation of the RT, model simulations quantify: (1) given an inhaled exposure, the degree or efficacy of antibody protection relative to the pre-immunity outcome of infection* versus *clearance probabilities; and, (2) given a successful infection, the efficacy of antibody protection relative to pre-immunity outcome on the subsequent progression of viral load and infected cells.*

The two mechanisms of antibody protection we explore are: *(1) neutralization*, widely perceived as the primary role of SARS-CoV-2 specific Ab (Klasse, 2014); and, *(2) muco-trapping*, whereby Ab cross-link viral spikes to mucin polymer domains in the mucosal barrier (Schaefer and Lai, 2022). For each mechanism, the model incorporates kinetic parameters for binding and unbinding rates as well as the quantity of potential trimeric binding sites on SARS-CoV-2 viruses (the number of spikes), which we shall show is an important determinant of Ab protection. For this paper, we specify several inputs to illustrate the capabilities of the model. The main inputs that will be varied are the nasal passage or lung generation number, absence of Ab, type of Ab present (neutralizing, muco-trapping, or bivalent neutralizing and muco-trapping), and the Ab concentration. Several other important parameters remain fixed in this work, including Ab-virion binding kinetic rates k_{on}, k_{off}, and the Ab-mucin affinity parameter, α. Other important SARS-CoV-2-specific parameters, including the virion production rate ν_{prod}, the duration of the eclipse phase $t_{latency}$, and probability of infection per virion-cell encounter p_{inf}, were studied in the pre-immunity model in (Pearson et al., 2022). While we expect similar outcome sensitivities to these parameters in the presence of Ab, those studies are for the future.

The model presented here incorporates mechanisms of Ab protection and the associated parameters that govern the strength of those mechanisms. Many of the Ab-virus and Ab-mucin polymer interactions have yet to be measured (if so, then not reported) with quantitative accuracy, and rarely at the scale of Ab-virus or Ab-mucin binding events in our agent-based model. One advantage and potential value of mathematical modeling, and a goal of this work, is to *predict which mechanisms and associated Ab interaction parameters are most influential in Ab protection, and in which situations* (e.g., *prevention or post onset of infection)*. We have not found published evidence for the differences in the physical properties of Ab produced by the immune system through vaccination, from prior exposure and infection, or from engineered monoclonal Ab use for inhalation therapy. By physical properties we mean the kinetic rates of Ab interactions with viruses and mucosal barriers to combat viral infection, essential information since Ab-virion and Ab-mucus interactions are not covalent, but transient, therefore governed by stochastic binding and unbinding events.

With estimates of the kinetic rates of Ab-spike binding and unbinding, we can determine the accumulation rate and equilibrium percentage of bound Ab to viral spikes, and how these key properties depend on local Ab concentration. With our model, from estimates of these kinetic rates, we quantify the widely cited mechanism of neutralization of infectious viral particles. In particular, we clarify that neutralization is a misnomer, since 100 % neutralization of a population of virions is virtually impossible; rather, this mechanism yields degrees of neutralization that fluctuate about some mean % of neutralization, i.e., % of spikes occupied by Ab and therefore unable to bind to cell receptors. Our model assesses the efficacy of neutralization as the source of Ab protection against SARS-CoV-2 viruses, and how the degree of efficacy depends on Ab concentration, Ab-spike binding and unbinding rates, and the number of spikes on SARS-CoV-2 viruses. Furthermore, we show that neutralization efficacy is generation-dependent in the human respiratory tract, and the efficacy is different for prevention of infection from initial exposure

versus protection post onset of infection. Given the documented mutations of spike structural proteins since early 2020, these Ab-spike kinetic rates have undoubtedly changed, just like the spike-receptor binding affinities have (Hui et al., 2022). Nonetheless, we repeat that we have yet to find published measurements of the change in these properties for different SARS-CoV-2 variants, which almost surely are different for infection-induced, vaccine-induced, and engineered Ab.

Another protective mechanism provided by Ab is via trapping of viruses in mucus—the ability of Ab to crosslink viruses in the mucus barrier by way of dual Ab binding affinities to viral spikes and to domains on the mucin polymers that comprise mucus (see below for more details and references). Viruses trapped in the mucus layer would be eliminated by the first line of respiratory defense from inhaled pathogens or toxic species: MCC to the esophagus to be swallowed into the acidic environment of the stomach (Matsui et al., 1998; Knowles and Boucher, 2002; Beule, 2010; Rygg and Longest, 2016). Our model allows us to answer an important question: from one or multiple modes of Ab protection against SARS-CoV-2, what are the Ab titers (count per unit volume), specific to the nasal tract, trachea (generation 0), and subsequent generations of the LRT, sufficient to minimize the risk of initial infection, to arrest existing infection, or to stem the tide of infection sufficiently so that other immune responses can overwhelm the infection?

Since the muco-trapping Ab-protection mechanism is far less recognized, we pause to cite previous work. Bi-specific Ab (induced by vaccines or infection or engineered and delivered via inhalation) have *binding affinities both to virion spikes and to mucin polymer domains*. Such Ab can thereby potentially crosslink virions within the mucosal barrier, dramatically lowering their diffusive transport, and empowering MCC. This Ab-crosslinking mechanism was shown, mathematically and experimentally, to be effective against HIV in vaginal mucus (Chen et al., 2014): the aggregation of virion-Ab-mucus crosslinks affords the strongest protection (far greater than neutralization alone), allowing time for natural clearance mechanisms to eliminate trapped virions. Effectiveness of muco-trapping of viruses by native and engineered Ab has been widely explored theoretically and experimentally (Chen et al., 2014; Chen et al., 2015; Wessler et al., 2016; Newby et al., 2017; Newby et al., 2018; Jensen et al., 2019; Xu et al., 2019; Schroeder et al., 2020), yet this potential protection mechanism has received little attention in the COVID-19 pandemic. Regdanvimab, a monoclonal Ab approved for use in the European Union, was recently reformulated as an inhaled therapy, IN-006 (McSweeney et al., 2022). IN-006 demonstrated the ability to reduce the effective diffusivity of SARS-CoV-2 particles by 10-fold in airway mucus through mucus crosslinking (Moench et al., 2022). In addition, IN-006 preserved strong binding affinities and neutralization potential. While the utilization of muco-trapping against SARS-CoV-2 has been limited so far, it has also been demonstrated effectively to fight against influenza (Wang et al., 2017), herpes (Wang et al., 2014), and has been shown to be a key component in ZMapp, the first drug to show excellent results in fighting the Ebola virus (Yang et al., 2018). These results motivate their inclusion in our post-immunity model platform.

2. Methods

The nasal passage and each lung generation is modeled as a 3-dimensional rectangular domain (unfolded cylinder) consisting of a rectangular grid of epithelial cells adjacent to a uniform, non-advecting $7\mu m$ PCL layer, adjacent to a mucus layer with variable thickness depending on the generation (Fig. 1). The air core presents the air-mucus interface where inhaled infectious seeds are initialized. (See Table 1 for lengths, mucus layer thicknesses, and advection velocities used in all simulations for each generation.) The epithelial cell grid consists of ~50 % infectable (primarily ciliated) cells (uniformly distributed). The movement of individual infectious virions shed from infected epithelial cells, infection of these cells, two states of infected cells (in the eclipse phase, followed by replication phase), replication of infectious virions at the cell-PCL interface, are then tracked over time.

Let x denote the radial, y the axial, and z the azimuthal coordinates of the system (Fig. 1C). Then $x = 0\mu m$ denotes the ASL-epithelial interface, $x = \mathrm{PCL_{gen}} = 7\mu m$ denotes the PCL-mucus interface, and $x = \mathrm{PCL_{gen}} + \mathrm{Mucus_{gen}}$ denotes the air-mucus interface. MCC results in advection in the y-direction for $x > \mathrm{PCL_{gen}}$(downward in the nasal passage, upward for all other generations). Then the virion equations of motion are given by the stochastic differential equations:

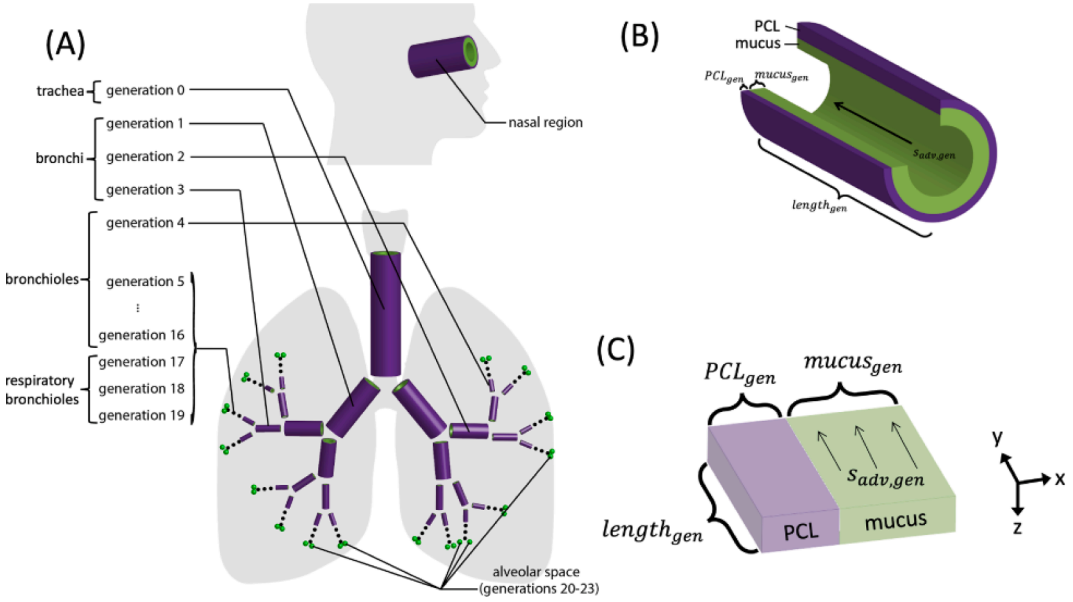

Fig. 1. Schematic of the RT (reproduced with permission from (Chen et al., 2022). (A) The nasal and lower RT network (excluding pharynx and larynx) idealized as cylinders plus the alveolar space. (B) Cylindrical airways are multi-layered: luminal airspace, mucus layer with variable thickness and advection velocity, uniform 7 μm, non-advecting, periciliary liquid layer (PCL), and epithelial cells / tissue. (C) The cylindrical generations can be locally unfolded to a rectangular geometry, with ×, y, and z coordinates as shown. Note: the ratio of mucus to PCL thickness shown is highly variable (See Table 2), so that B and C are loosely representative of generation 10 of the lower RT.

Table 1
Physical dimensions per generation (abbreviated Gen, Column 1) of the nasal and lower RT airways, mucus layer thickness, advection velocity by MCC, and the resulting time to clear from the generation.

Gen	Length [mm]	Mucus layer thickness [μm]	Mucus layer advection [mm/min]	Time for mucus layer to advect the full length [hrs]
Nasal	1.30×10^2	17.0	8.8000	0.2462
0 Trachea	1.00×10^2	50.0	5.5000	0.3030
1	4.36×10^1	44.4	3.9100	0.1858
2	1.78×10^1	38.8	2.4900	0.1191
3	9.65×10^0	33.1	1.5400	0.1044
4	9.95×10^0	27.5	0.8890	0.1865
5	1.01×10^2	21.9	0.4960	0.3394
6	8.90×10^1	19.6	0.2960	0.5011
7	9.62×10^0	17.3	0.1670	0.9601
8	8.67×10^0	15.0	0.1010	1.4307
9	6.67×10^0	12.7	0.0616	1.8047
10	5.56×10^0	10.4	0.0396	2.3401
11	4.46×10^0	9.32	0.0252	2.9497
12	3.59×10^0	8.29	0.0165	3.6263
13	2.75×10^0	7.26	0.0113	4.0560
14	2.12×10^0	6.23	0.0080	4.4444
15	1.68×10^0	5.20	0.0057	4.9296
16	1.34×10^0	4.70	0.0041	5.4739
17	1.20×10^0	4.21	0.0028	7.0671
18	9.20×10^{-1}	3.72	0.0014	11.0312
19	8.00×10^{-1}	3.22	0.0010	13.8889
20	7.00×10^0	2.73	0.00063	18.5185
21	6.30×10^0	2.44	0.0000	———
22	5.70×10^{-1}	2.16	0.0000	———
23	2.50×10^{-1}	1.87	0.0000	———

$$dx = \sqrt{2D_v}dW_1$$

$$dy = \sqrt{2D_v}dW_2 + s_{adv,gen}1_{\{x>PCL_{gen}\}}dt$$

$$dz = \sqrt{2D_v}dW_3$$

where $s_{adv,gen}$ is the advection velocity in the generation, and W_1, W_2, W_3 represent 1-dimensional Brownian motion.

When a virion within the ASL (PCL plus mucus) encounters an infectable epithelial cell at $x = 0$, infection occurs with probability $p_{inf} = 0.3$ and the virion is removed from the ASL, otherwise the virion is reflected back into the PCL; encounters with non-infectable cells also have reflective boundary conditions. These boundary conditions ensure that virions that do not have an infection event remain in the ASL. Newly infected cells undergo a period of latency (the eclipse phase) during which virion RNA is assembled and RNA copies are replicated. The infected cell then exits the eclipse phase, and the shedding phase begins as soon as infectious virion progeny start getting shed into the ASL at a rate of $\nu_{prod} = 2000$virions/day (estimate in (Chen et al., 2022) for the alpha variant). At $x = PCL_{gen} + Mucus_{gen}$, the air-mucus interface, some virions may become entrained in aerosolized droplets and thus removed from the system. In this work, we do not account for infectious virion removal by aerosolization, and thus impose reflecting boundary conditions. We refer to (Chen et al., 2022) for further details on the modeling equations, including diffusion of virions, geometry of the lung, MCC advection velocity per generation, the infection kernel, viral replication algorithm, and simulation details.

We next describe antibody kinetics and their effect on infection probabilities and virion motion (refer to Fig. 2). We assume each SARS-CoV-2 spike can bind up to three Ab. Individual Ab bind and unbind independently with rates k_{on} and k_{off}. Several SARS-CoV-2 k_{on} and k_{off} values are given in Table S1; we choose values in the middle range of reported values (See Table 2 and (Li et al., 2020), those associated with IgG1 ab1. Overall binding rates depend on the number of unoccupied sites $3N_* - n$, where n is the number of Ab already bound, and N_* is the number of spikes on a SARS-CoV-2 virion, estimated at $N_* = 24 \pm 9$ (Ke et al., 2020; Laue et al., 2021). Individual Ab diffuse rapidly relative to virions; the Ab concentration is thus assumed to be at spatial equilibrium. Additionally, local individual Ab counts through all simulations remain much larger than local virion counts, such that Ab concentration changes by binding and unbinding events are minor enough for Ab concentrations to be assumed constant regardless of the number of binding or unbinding events that occur.

We model neutralization as a reduction in viral infectivity by binding Ab. Each bound Ab is assigned a spike, and we assume one bound Ab sufficient to block the infectivity of the spike. Thus, binding additional Ab to the same spike does not affect infectivity. This assumption is easily modified given experimental evidence, and we note this assumption amplifies protection due to neutralization if two or even three occupied spike domains are required to block spike binding to cell receptors.

Muco-trapping Ab also have a (relatively weaker) binding affinity to mucins, and the mucin-Ab affinity is estimated by comparing Ab diffusivity in mucus with its diffusivity D_{Ab} $40\mu m^2/s$ (See Table 2) in buffer, resulting in a knockdown factor α 80% (See Table 2 and (Schaefer and Lai, 2022; Chen et al., 2014; Jensen et al., 2019). In mucus, we model this affinity by considering two populations of Ab: $u_f(\vec{x}, t)$ is the *concentration of free Ab* (not interacting with mucins) near position $\vec{x}$ at time t, and $u_b(\vec{x}, t)$ is the *concentration of Ab interacting with mucins*. Ab interact with an individual virion V via the kinetic equation.

$$(\mathrm{Ab}) + (\mathrm{Ab})^n V \leftrightharpoons (\mathrm{Ab})^{n+1} V$$

The reaction rates depend on whether the Ab is freely diffusing or interacting with mucins, since the Smoluchowski encounter rate is greatly reduced for mucin-interacting Ab. The relative diffusivity of virions and mucin-interacting Ab is reduced from $D_{Ab} + D_v$ to D_v for bound Ab, and the binding rate is reduced proportionally. Thus, the binding rate for mucin-bound Ab (k^b_{on}) to virions is $k^b_{on} = \frac{D_v}{D_{Ab}+D_v}k_{on} \approx \frac{1}{30}k_{on}$. Assuming that Ab bind to each of the $3N_*$ sites independently, the kinetic equations for the entire virion thus have a forward rate of $(3N_* - n)\left(k_{on}u_f(V(t), t)\right) + k^b_{on}u_b(V(t), t)$ and a reverse rate of $(n+1)k_{off}$, where n represents the number of sites with a bound Ab.

Since Ab diffuse much more rapidly than virions, the Ab concentration is assumed to be at steady state at the model time scale. Solving the diffusion equation yields a constant solution for $u_f(\vec{x}, t)$, and

$$u_b(\vec{x}, t) = \begin{cases} 0 & \text{for } \vec{x} \text{ in PCL} \\ \dfrac{1-\alpha}{\alpha}u_f(\vec{x}, t) & \text{for } \vec{x} \text{ in mucus} \end{cases}$$

Since $u_f(\vec{v}, t) + u_b(\vec{v}, t) = [\mathrm{Ab}]$, the total Ab concentration, $u_f(\vec{x}, t) \equiv \frac{\alpha(\mathrm{PCL+Mucus})}{\alpha \mathrm{PCL+Mucus}}[\mathrm{Ab}]$.

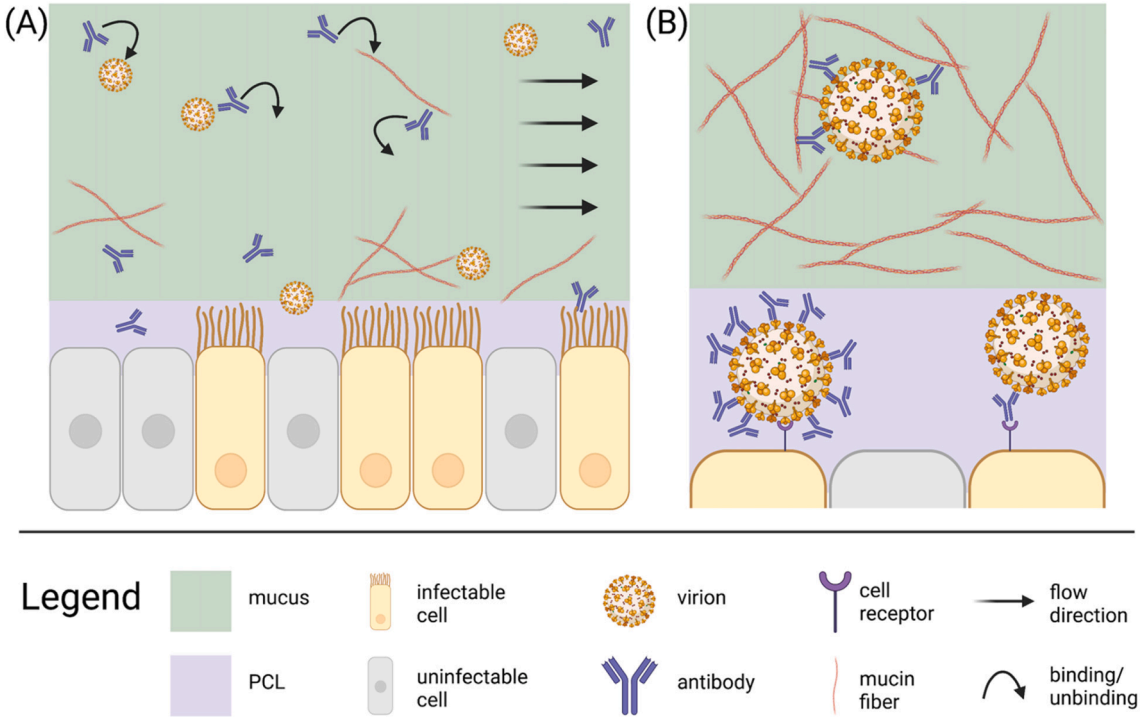

Fig. 2. Schematic of ASL environment. (A) Virions, Ab, and mucins inhabit the ASL (mucus and PCL). Fab arms of Ab bind to and unbind from virion spikes, while the Fc domain of Ab more weakly bind to and unbind from mucins. (B) Virions may become trapped in the mucin network via Ab-spike-mucin crosslinks.

Table 2
Base parameters and values in the model.

Parameter	Description	Value	Reference
D_v	Base virion diffusion coefficient	$1.27\mu m^2/s$	(Lai et al., 2009)
PCL_{gen}	Thickness of the PCL layer	$7\mu m$	(Chen et al., 2022)
$Mucus_{gen}$	Thickness of the mucus layer in generation	Variable (See Table 1)	(Chen et al., 2022)
$s_{adv,gen}$	Advection velocity in generation	Variable (See Table 1)	(Chen et al., 2022)
ν_{prod}	Infectious virion production rate	2000 virions/ day	(Chen et al., 2022)
$t_{latency}$	Duration of eclipse phase	12 hrs	(Chen et al., 2022)
$c_{infectable}$	% Infectable cells	50 %	(Chen et al., 2022)
p_{inf}	Probability of infection per encounter	0.3	(Chen et al., 2022)
N_*	Number of spikes on virion	24	(Ke et al., 2020)
D_{Ab}	Base Ab diffusion coefficient	$40\ \mu m^2/s$	(Olmsted et al., 2001; McKinley et al., 2014)
k_{on}	Ab association rate	2.40e5 $M^{-1}s^{-1}$	(Li et al., 2020); Table S1
k_{off}	Ab dissociation rate	4.00 e-5 s^{-1}	(Li et al., 2020); Table S1
α	Ab-mucin affinity	0.8	(Chen et al., 2014; Schaefer and Lai, 2022)

Ab-mucin binding interactions are much faster than the model time scale, so the diffusion coefficient for virions can be simplified as $\alpha^n D_v$. From this reduced diffusion coefficient, it is apparent that with many bound Ab, a virion is essentially immobilized, even with a modest α, empowering the protection afforded by natural mucus clearance in the respiratory tract for SARS-CoV-2. These analyses underscore the critical need to know, if necessary to engineer, the dual binding affinities of Ab (Ab-virion affinity and Ab-mucin affinity), as well as the Ab concentrations at every location in the RT, since this promises to dramatically enhance Ab protection (Lai et al., 2021; Cruz-Teran et al., 2021). We also discuss below the role played by the unusually small number of SARS-CoV-2 spikes, N_*.

3. Results

We performed simulations which directly compared the effectiveness of different protective mechanisms provided by Ab. In order to do this, we ran simulations under several conditions. First, Ab were not present, the pre-immunity condition. Second, Ab were allowed to "neutralize" virions but not trap, i.e., Ab bind to and accumulate on virion spikes, inhibiting the ability of spikes to bind to infectable target cells. We call attention to the fact that the degree of neutralization is determined by the percentage of Ab-bound spikes, since the remaining unoccupied spike trimers are available to bind to cell receptors. Since Ab-receptor binding is transient and not covalent, depending on Ab concentration it takes time (see Fig. 3, Panels (A), (C)) to converge to the quasi-equilibrium saturation % of Ab-occupied spikes, in which time many virions will have already infected cells. Furthermore, the saturation value is not 100 %. Third, Ab were allowed to both neutralize and muco-trap virions. From these different conditions, we show the efficacy due to neutralization across various scenarios; we further show muco-trapping, if also conveyed by the Ab in question, offers enhanced protection over neutralization.

3.1. Muco-trapping by neutralizing Ab dramatically reduces virion-epithelial cell encounters and infection in the nasal passage

Fig. 3 shows example paths of virions undergoing diffusion through the nasal passage under two hypotheses: Ab that only neutralize virion spikes and Ab that both neutralize and muco-trap. Although a large reduction in infectivity (down to ~ 6 % of the original infectivity) occurs within 10 min of exposure to neutralizing Ab, the proximity of virions to many infectable cells and the high base infectivity will result in a large number of virions infecting before this time window (Panels (A), (B)), and many virions after this window still retain sufficient infectivity to infect cells (Panels (C), (D)). In contrast, muco-trapping Ab can

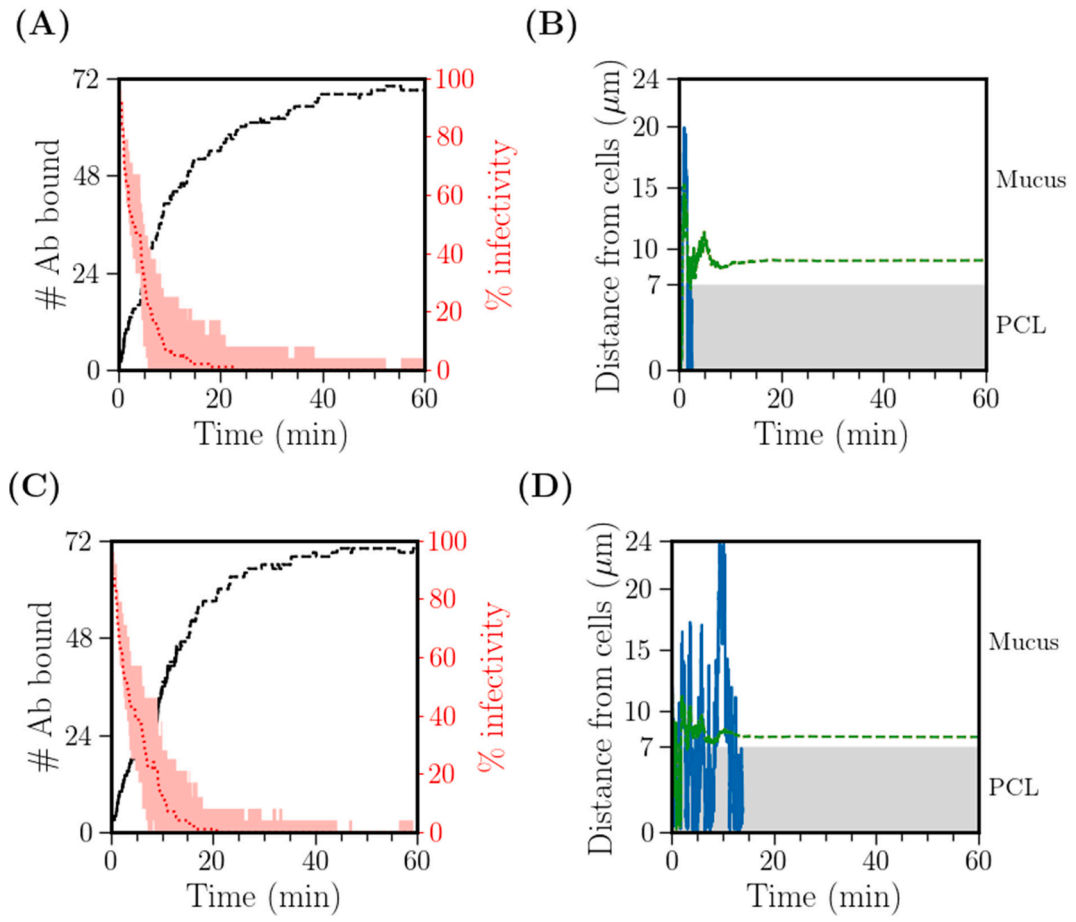

Fig. 3. Dynamics of SARS-CoV-2 virions shed from infected epithelial cells in the nasal passage. (A) and (C) Ab bound to the virion over time is in black, with the corresponding mean infectivity displayed as a dashed red curve, with the red shaded region indicating the infectivity range (for the neutralizing case) over 10^4 trials in assigning Ab to the $N_* = 24$ spikes. (B) and (D) show the distance to epithelial cells over time for (blue) neutralizing Ab and (green) both neutralizing and muco-trapping Ab. $k_{on} = 2.40\text{e}5\ M^{-1}s^{-1}$, $k_{off} = 4.00\ \text{e-}5\ s^{-1}$, $\alpha = 0.8$, $[Ab] = 1\mu g/mL$.

effectively immobilize a virion with even a modest number of virion-bound Ab. After 5 min, close to 26 Ab will have accumulated on the virion surface, reducing virion diffusivity by 99.7 %.

To further illustrate the protection offered by muco-trapping, we looked at how this mechanism limits virion-target cell encounters, and thus limiting infection. Fig. 4 shows the spatial distribution of virions after 1 hr of simulation time for virions that have not infected cells. With neutralizing Ab, the distribution is relatively uniform throughout both the PCL and mucus (Panel (A)). However, with muco-trapping Ab, virtually no virions remain in the PCL, with the overwhelming majority having been trapped in mucus near the PCL interface. In both cases, many virions have infected cells. With neutralizing Ab, virions will

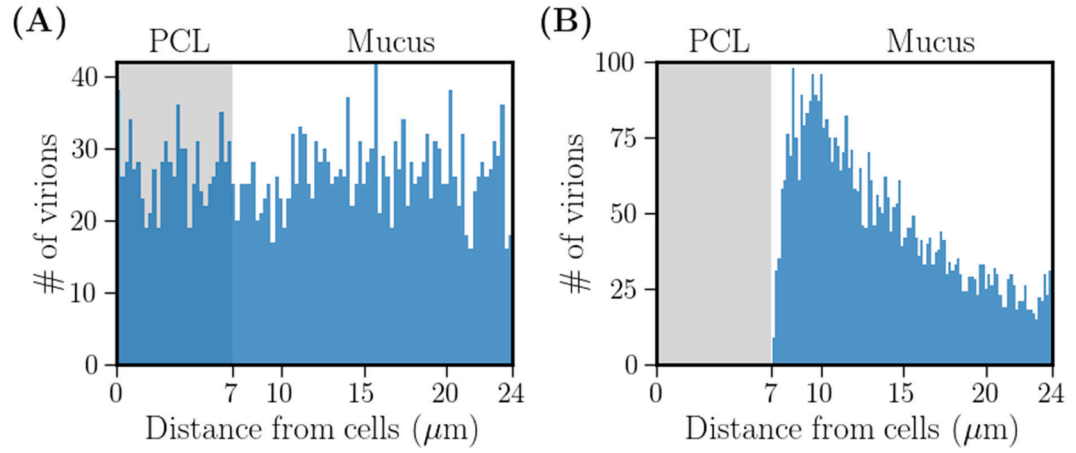

Fig. 4. Distribution of virions by distance to epithelial cell layer shed into the nasal passage after 1 h with (A) neutralizing Ab, (B) both neutralizing and muco-trapping Ab, $k_{on} = 2.40\text{e}5\ M^{-1}s^{-1}$, $k_{off} = 4.00\ \text{e-}5\ s^{-1}$, $[Ab] = 1\mu g/mL$. For muco-trapping, Ab-mucin affinity parameter $\alpha = 0.8$. Virions originated at the epithelial-ASL interface.

continue to infect cells at later times, when the virions will also have been advected to locations with a large percentage of uninfected cells. However, with muco-trapping Ab, almost all virions infecting cells will have infected them earlier and thereby "closer" than non-muco-trapping Ab. These infections are thus likely to occur nearer the original location of shedding, thus limiting the infection horizon.

3.2. Target cell infections from inhaled exposures throughout the respiratory tract are more likely with neutralizing Ab than with muco-trapping Ab

We compared statistics for all target-cell infections versus generation, presented in Fig. 5. Mean population data for the nasal passage and lung generations are displayed in Table 1, including the length of the generation, mucus layer thickness, and advection velocity, and the resulting time to clear from the generation. Each generation also includes a $7\mu m$ PCL. For each generation, 10^4 realizations of virions deposited initially in the middle two quartiles of each generation at the air-mucus interface are then simulated until infection or clearance for a maximum of 24 h. Fig. 5 displays the probabilities of infection for four different Ab cases: no Ab, neutralizing only, muco-trapping only, and a combination of neutralizing and muco-trapping Ab. Error bars, indicating the 95 % confidence intervals, for each simulation set were calculated using the theoretical standard deviations for the binomial random variable.

Neutralizing Ab provide a degree of protection against infection from inhaled exposure, and the degree is clearly generation-dependent as revealed when comparing the curves for "No Ab" vs "Neutralizing Ab," from cutting in half the finite probabilities within the nasal and upper generations of the LRT, to lowering absolute infection to finite probabilities in the deep lung. By contrast, *many virions crosslinked by muco-trapping Ab experience a rapid diffusivity knockdown before they are able to diffuse across mucus to the PCL*, where muco-trapping is less potent. The large reduction in infections due to muco-trapping is clear; muco-trapping provides a substantial reduction in infections from either no Ab or neutralizing Ab, and the addition of neutralization provides limited additional protection. We especially call attention to the striking effect of neutralizing and muco-trapping Ab, and in particular to the dramatic protection against infection in the nasal passage and upper generations of the lower RT. The likelihood of infection in the nasal tract drops from 670 per 1000 exposures in the middle two quartiles without Ab protection, to 395 per 1000 exposures with neutralizing Ab, to 47 per 1000 exposures with neutralizing and muco-trapping Ab! *Coupled with the clinical insights in* (Hou et al., 2020) *and model simulation results in* (Chen et al., 2022)*, strongly indicating that nasal and nasopharyngeal infections are the likely source of self-transmission of infection to the deep lung, the powerful protection provided by neutralizing and muco-trapping Ab from nasal exposure and protection is evident.* Similar conclusions can be drawn for the trachea and other lung generations.

Figure S1 displays cumulative probabilities for a virion originating in a particular generation to infect the lung airways (in any generation). An open problem in lung mechanics is positioning a virion along the PCL-mucus (radial) axis when transitioning between generations. MCC transports upward in the LRT, so when two generations converge from generation k to generation $k-1$, the mucus layers collide at the junction and reassemble to form one mucus layer that is slightly thicker. In the simulations for Figure S1, we assume that the location in the new generation is proportional to its location in the previous generation (not including the PCL). That is, $\frac{x_{\text{gen,new}}-\text{PCL}_{\text{gen,new}}}{\text{Mucus}_{\text{gen,new}}} = \frac{x_{\text{gen,prev}}-\text{PCL}_{\text{gen,prev}}}{\text{Mucus}_{\text{gen,prev}}}$. With some notable exceptions, the probabilities are almost identical to those in Fig. 5. In the absence of Ab, there is a large increase in the cumulative probability to infect for generations 1–7 (upper branches of the LRT), since many virions are cleared out of their generation of origin but are unlikely to traverse all remaining generations and the trachea (generation 0), then into the esophagus and stomach. For higher numbered generations, i.e., down farther in the LRT, the MCC velocity, thickness of the mucus layer, and total length of the branch all progressively drop, ensuring that virions will almost always infect within their generation of origin. For neutralizing Ab, there is again a small difference in the cumulative probability to infect in generations 1–6 as some virions that clear out of the generation of origin infect the next generation. However, with muco-trapping Ab, virions that are cleared from the generation of origin have generally become entrained in the mucus escalator, with enough Ab to be crosslinked to the mucin network. Such muco-trapped virions will generally be completely cleared by MCC (or remain immobilized within mucus within generations farther down in the LRT). (While not modeled here, muco-trapped virions also become prime targets for adaptive immune response agents, e.g., macrophages, or antiviral drugs.).

Fig. 6 shows infection maps resulting from an initial shedding cell at the upstream end of the nasal passage. Advection strongly biases the spread of infectious virions downward in the nasal passage toward the nasopharynx, resulting in a slowly widening (due to diffusion transverse to mucus advection) streak of infection downstream (Panel (A) without Ab as previously reported in (Chen et al., 2022), and Panel (B) with neutralizing Ab). This effect is dramatically disrupted by the action of muco-trapping Ab, however, Panels (C) and (D), as a large percentage of virions are being advected within the mucus escalator, where they

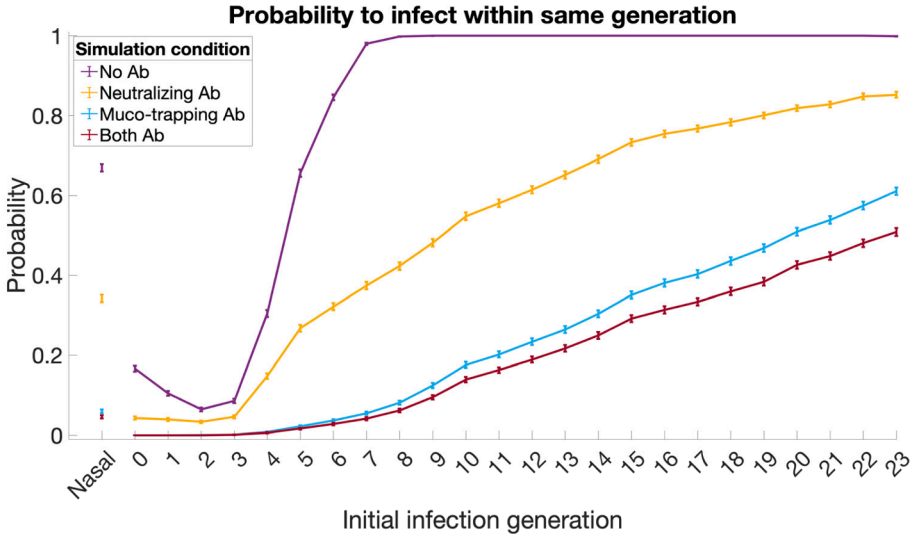

Fig. 5. Model-simulated infection probabilities from inhaled virions at the air-mucus interface ($x = \text{PCL}_{\text{gen}} + \text{Mucus}_{\text{gen}}$) to infect within that generation. Averages are over 10^4 virions shed by infected cells at the epithelium-ASL interface and uniformly distributed within the middle two quartiles of the nasal passage, trachea, and all lower lung generations): for no Ab, neutralizing Ab only, muco-trapping Ab only, and Ab that are both neutralizing and muco-trapping. In each case, $k_{\text{on}} =$ 2.40e5 $M^{-1}s^{-1}$, $k_{\text{off}} =$ 4.00 e-5 s^{-1}, $[Ab] = 1\mu g/mL$. For muco-trapping, Ab-mucin affinity parameter $\alpha = 0.8$. Virions not infecting within 24 h were assumed not to infect. Error bars indicate the 95 % confidence intervals in the simulations of the probabilities.

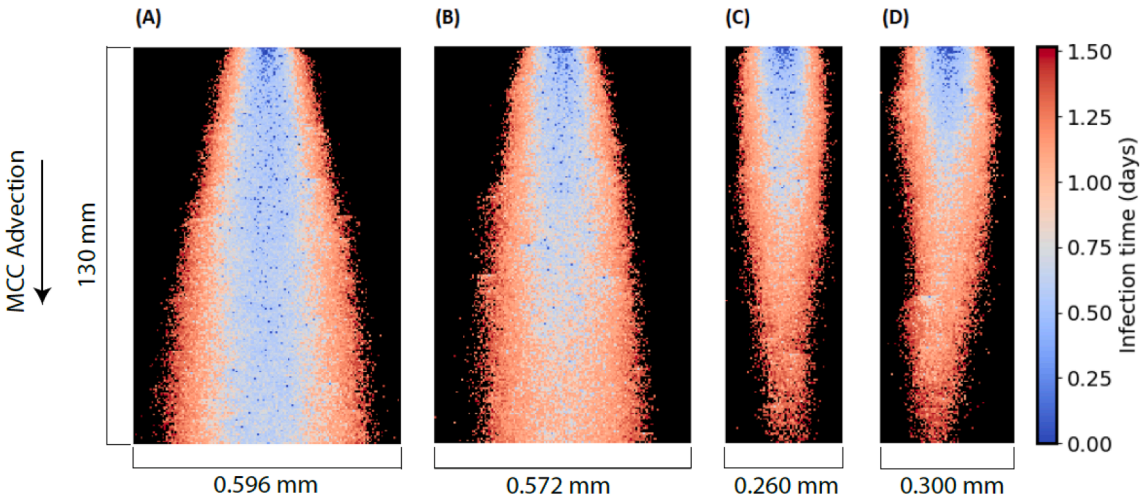

Fig. 6. Snapshots of the spread of infected nasal epithelial cells in the first 36 h originating from a single infected and shedding cell at the entry of the nasal passage with various types of Ab. (A) No Ab, (B) Neutralizing Ab, (C) Muco-trapping Ab, (D) Both neutralizing and muco-trapping. $k_{on} = 2.40e5\ M^{-1}s^{-1}$, $k_{off} = 4.00$ e-5 s^{-1}, $[Ab] = 1\mu g/mL$. For muco-trapping, Ab-mucin affinity parameter.$\alpha = 0.8$.

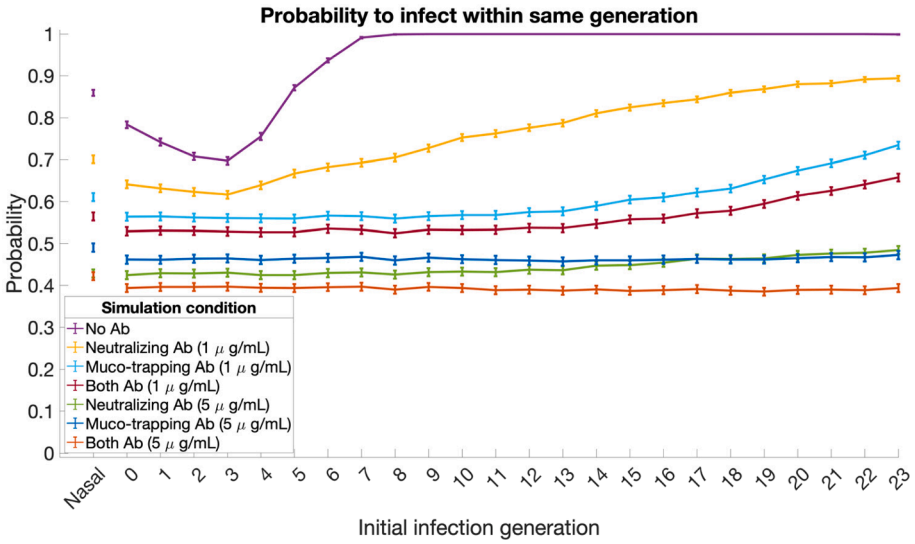

Fig. 7. Model-simulated infection probabilities from shed virions at the epithelial-ASL interface ($x = 0\mu m$) to infect within that generation. Averages are over 10^4 virions shed by infected cells at the epithelium-ASL interface and uniformly distributed within the middle two quartiles of the nasal passage, trachea, and all lower lung generations): for no Ab, neutralizing Ab only, muco-trapping Ab only, and Ab that are both neutralizing and muco-trapping, for two different Ab titers: [Ab] = $1\mu g/mL$ and $5\mu g/mL$. In each case, $k_{on} = 2.40e5\ M^{-1}s^{-1}$, $k_{off} = 4.00$ e-5 s^{-1}. For muco-trapping, Ab-mucin affinity parameter $\alpha = 0.8$. Virions not infecting within 24 h were assumed not to infect. Error bars indicate the 95 % confidence intervals in the simulations of the probabilities.

approach equilibrium saturation of spike-Ab-mucin crosslinks, effectively immobilizing the virions in the mucus escalator. Fig. 6 *illustrates the powerful enhancement of MCC provided by the combination of neutralizing and muco-trapping Ab!* We note that the resulting nasal viral titer is thereby substantially smaller with muco-trapping Ab versus neutralizing Ab or no Ab. Indeed, *with a sufficiently high Ab concentration, the downstream infection can be completely arrested* (Fig. 8(C), (D)).

Fig. 7 plots simulated infection probabilities throughout the respiratory tract following a successful infection event. In this scenario, virions are initialized at the PCL-cell interface as they are shed from infected cells. While the probabilities for infection are obviously greater than with virion deposition at the air-mucus interface, *at moderate Ab concentrations*, Fig. 6 and Fig. 7 (1 $\mu g/mL$), *muco-trapping still provides noticeable added protection over neutralization, both to prevent infection and to limit the spread of infection. Interestingly, at higher Ab concentrations (*Fig. 7 *(5 $\mu g/mL$) and* Fig. 8*), the probabilities for infection become comparable for neutralization and muco-trapping, and in some generations, favor neutralizing Ab, and either or both mechanisms substantially limit the spread of infection.* However, we caution Table S2 reveals that in the neutralizing case, many virions simply transport longer before infecting, thereby spreading the infection farther and increasing the number of cells that are ultimately infected. Figure S2 likewise displays plots of cumulative probabilities to infect (analogously to Fig. 5 and Figure S1) the entire respiratory tract with very similar effects: a large increase in the cumulative probability without Ab, and a modest increase with neutralizing Ab.

3.3. Sensitivity analysis

In this section, we explore ranges for several key parameters in this model. For these parameters, there may be a wide range in the feasible set of values due to limited laboratory and clinical measurements, potential differences between ex vivo and in vivo outcomes of infection, uncertainty in the literature, differences in variants, or differing Ab properties. The sensitivity analysis here elucidates the effects that these ranges will have on the viral load.

3.3.1. Viral and Ab diffusivity

The Stokes-Einstein diffusivity of a virion in water at 37 °C with diameter 100 nm is $6.57\mu m^2/s$, which is the upper bound for the diffusivity of a virion in mucus. While viruses have generally evolved to diffuse readily through mucus, variability has been reported, with 1.27

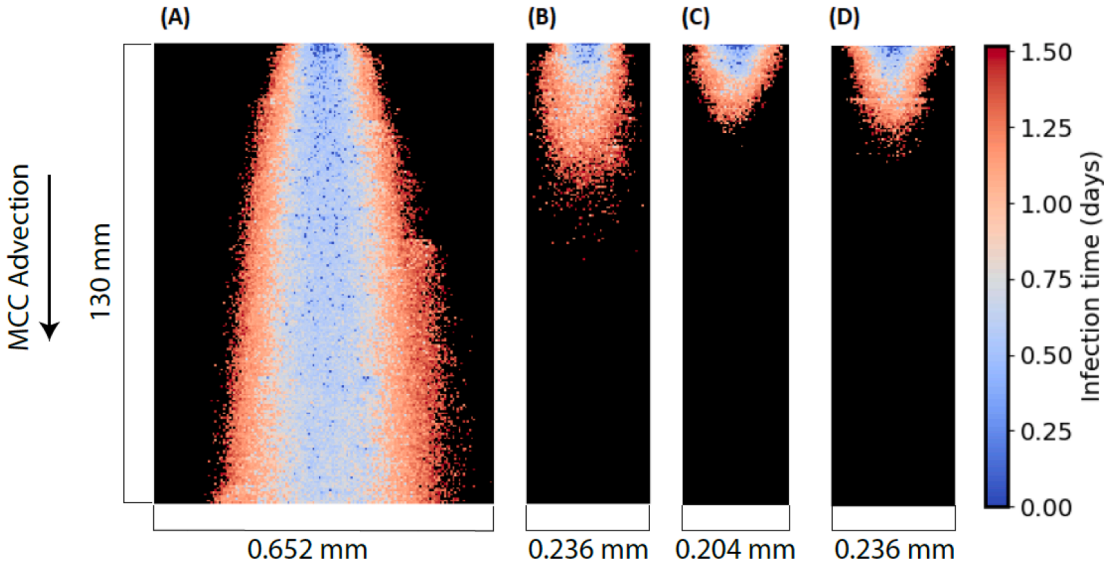

Fig. 8. Snapshots of the spread of infected nasal epithelial cells in the first 36 h originating from a single infected and shedding cell at the entry of the nasal passage with various types of Ab. (A) No Ab, (B) Neutralizing Ab, (C) Muco-trapping Ab, (D) Both neutralizing and muco-trapping. k_{on} = 2.40e5 $M^{-1}s^{-1}$, k_{off} = 4.00 e-5 s^{-1}, [Ab] = 5$\mu g/mL$. For muco-trapping, Ab-mucin affinity parameter.α = 0.8.

$\mu m^2/s$ for HIV in cervicovaginal mucus (Lai et al., 2009) and 0.23 $\mu m^2/s$ for SARS-CoV-2 in airway mucus (Moench et al., 2022). Fig. 9 (first two sets of bars) shows the viral load when varying virus diffusivity. Increasing virus diffusivity leads to greater horizontal spread of the infection front and thus a modestly higher viral load, while a decrease leads to a lower viral load. More dramatic protection afforded by Ab occurs at the lower diffusivity level (0.23 $\mu m^2/s$) with a 5-fold reduction in the viral load, while only a 2-fold reduction occurs at the higher diffusivity level (6.57 $\mu m^2/s$). This is likely due to the fact that more Ab are able to accumulate on virions before they are able to travel farther in the former case, thus compounding Ab-induced protection.

Ab diffusivity likewise is lower than the Stokes-Einstein value. However, it is likely to remain closer to its theoretical value in water, due to its smaller size relative to mucin pores. A reasonable lower bound is thus 18.5 $\mu m^2/s$ in mucus (Saltzman et al., 1994; Jøssang et al., 1988). In this work, however, Ab concentration is assumed to be at equilibrium, reflecting the rapid diffusivity of Ab. Thus, the only effect of changing the Ab diffusivity is a slight change in the binding rate equations. Unsurprisingly, the viral loads remain virtually unchanged from the base case (Fig. 9 (third set of bars)).

3.3.2. Virion production rate

The infectious virion production rate v_{prod} has a high degree of uncertainty due to it usually being estimated from total infectious virions, total RNA copies, and the ratio between them (Sender et al., 2021). Thus, estimates of v_{prod}have varied from 10 (Sender et al., 2021) up to 1000 (Moses et al., 2021). Furthermore, the literature on the Epsilon and Delta variants suggests that the infectivity ratio has increased 6-fold in comparison with Alpha (Despres et al., 2022). We have tested several additional values for v_{prod}in the relevant range (100, 500, 1000). Fig. 10 shows that our model (and indeed all models) are highly sensitive to this parameter, suggesting that further experimentation to measure the infectious virion production rate is extremely important.

3.3.3. Ab type

A table of SARS-CoV-2 Ab kinetic rates is presented in Table S1. To demonstrate the effect of these rates, we ran simulations with k_{on}, k_{off} associated with two other Ab types, chosen at the extreme ranges for each parameter. Fig. 11 shows that with the lowest k_{on} and highest $k_D = \frac{k_{off}}{k_{on}}$ among the reported Ab, C1A-g1 unsurprisingly elicited lower protection than from the base parameter set, with viral loads nearly identical to the case where no Ab are present. In contrast, with the highest k_{on} and lowest k_D, S103F(H)-S33R(L) elicited strong protection in all cases. Somewhat surprisingly, neutralizing Ab alone showed the largest reduction in viral load. Due to its high affinity, many Ab accumulate quickly on the surface of virions. Neutralizing Ab lower the probability of infection drastically. As a consequence, virions often do not infect nearby cells, but some eventually infect cells far away from the shedding

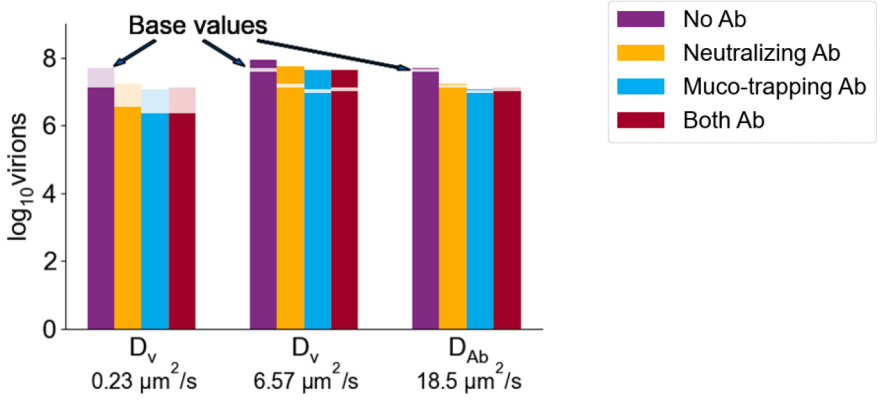

Fig. 9. Viral load sensitivity to changes in diffusivity. Viral load after 36 h originating from a single infected and shedding cell at the entry of the nasal passage with base parameters, except for viral diffusivity D_v, set to 0.23 $\mu m^2/s$ or 6.57$\mu m^2/s$ (first two sets of bars), and Ab diffusivity D_{Ab}, set to 18.5 $\mu m^2/s$ (third set of bars). The viral load from simulations for the base set of parameters for "No Ab," "Neutralizing Ab," "Muco-trapping," and "Both neutralizing and muco-trapping," are shown for comparison.

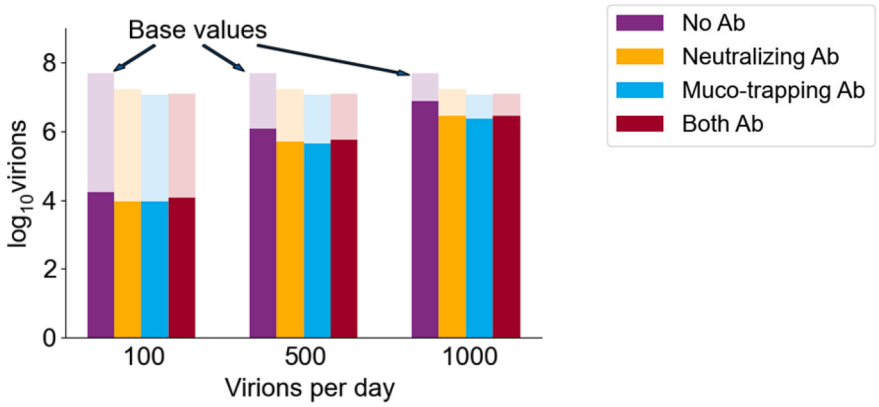

Fig. 10. Viral load sensitivity to changes in virion product rate. Viral load after 36 h originating from a single infected and shedding cell at the entry of the nasal passage with base parameters, except for virion production rate v_{prod}, set to 100, 500, 1000 $\text{cell}^{-1}\text{day}^{-1}$. The viral load from simulations for the base set of parameters for "No Ab," "Neutralizing Ab," "Muco-trapping," and "Both neutralizing and muco-trapping," are shown for comparison.

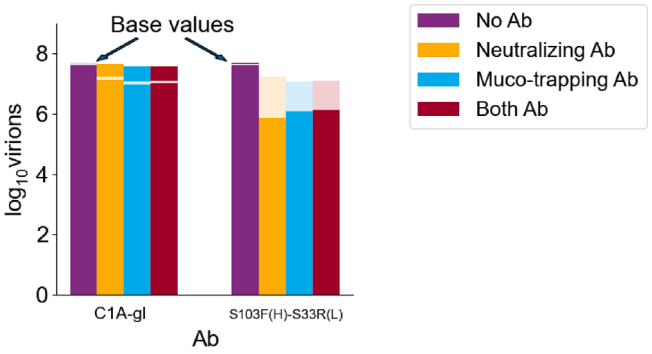

Fig. 11. Viral load sensitivity to changes in Ab kinetic rates. Viral load after 36 h originating from a single infected and shedding cell at the entry of the nasal passage with base parameters, except for Ab kinetic parameters k_{on}, k_{off}. For C1A-g1, $k_{on} = 4.41e4\ M^{-1}s^{-1}$, $k_{off} = 5.59\ e\text{-}3\ s^{-1}$; for S103F(H)-S33R(L), $k_{on} = 2.28e6\ M^{-1}s^{-1}$, $k_{off} = 2.28\ e\text{-}3\ s^{-1}$. The viral load from simulations for the base set of parameters for "No Ab," "Neutralizing Ab," "Muco-trapping," and "Both neutralizing and muco-trapping," are shown for comparison.

site. Interestingly, this leads to more separated seeding for future infections, and with more simulation time, neutralizing Ab eventually yield a higher infected cell count (and thus viral load). Indeed, after 60 h of simulation time, the infected cell count for neutralizing Ab is 2-fold higher than the infected cell count for muco-trapping Ab.

3.3.4. *Lung generation*

Many within-host models have focused on the URT (and especially the nasal passage) due to its role as the primary site of infection and driver of between-host transmission (Carruthers et al., 2022). However, a stronger understanding of infection dynamics in the LRT is important, especially insights into the development of severe infection (Moses et al., 2021; Chen et al., 2022). In Fig. 12, Gen 0 (the trachea) generates a similar viral load as that of the nasal passage, since the parameters (MCC advection speed $s_{\text{adv, gen}}$, generation length, and mucus thickness $\text{Mucus}_{\text{gen}}$) are relatively similar. *For generations farther down in the LRT, however, an unexpected result occurs, with neutralizing Ab creating higher infection than without Ab.* This effect can be traced to the minimal MCC in these generations. Without the advection provided by MCC, virions generally only infect nearby cells. However, as neutralizing Ab reduce the infectivity of virions, they travel farther before infecting, leading to a faster infection front. This suggests that muco-trapping, and not neutralization, may provide a better protection mechanism in the deep lung.

4. Conclusion

Protection against viral infections conveyed by Ab is widely attributed to neutralization (Klasse, 2014). Neutralizing Ab play an important role in blocking virion infection of epithelial cells, and many neutralizing Ab have been discovered or engineered against a wide variety of viruses. However, significant protection against viral infection has also been found with non-neutralizing Ab or even with Ab titers too low for sufficient neutralization (Moog et al., 2014; Hessell et al., 2009; Rerks-

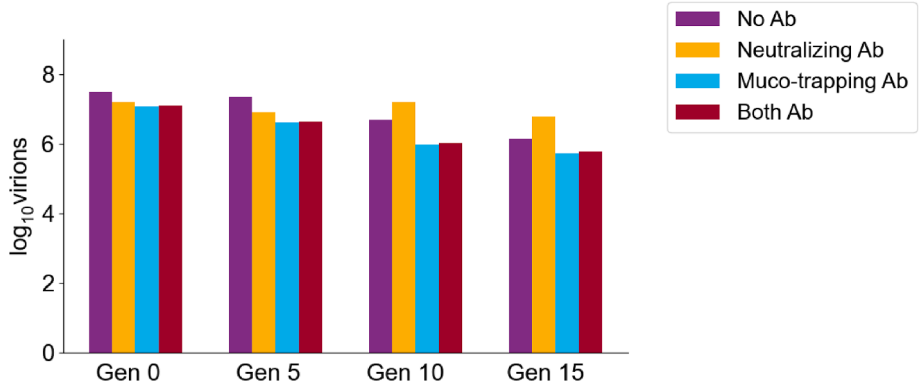

Fig. 12. Viral load sensitivity changes in lung generation. Viral load after 36 h originating from a single infected and shedding cell at the entry of lung generations 0 (trachea), 5, 10, 15, for four cases with base parameters as in previous figures: no Ab, neutralizing Ab, muco-trapping Ab, and neutralizing plus muco-trapping Ab.

Ngarm et al., 2009). These results suggest that other mechanisms play a significant role in protection against viral infection.

The present paper adds to a growing body of research demonstrating that muco-trapping, the powerful additional protection conveyed by Ab that also weakly bind to mucin polymer domains, is one of these mechanisms. The simulations, even at low Ab titers and for low Ab-mucin affinity, demonstrate the effectiveness of muco-trapping Ab in hindering initial infections and in slowing the spread of the infection front. At higher Ab titers, the infection is largely arrested. For Ab that combine both neutralization and muco-trapping, the effect can be synergistic. The neutralizing property may block early infection of cells, allowing for more Ab to accumulate; then muco-trapping immobilizes virions, allowing MCC to clear the infection.

Future studies will illuminate the most influential parameters and mechanisms providing greater protection. For example, in (McKinley et al., 2014), it was shown that the fast time scale of virion diffusion and infection implies that for in vivo protection, it is essential to bind as many Ab as possible quickly, even at the cost of a strong equilibrium number of bound Ab suggested by many *ex vivo* studies. That is, high k_{on}, rather than low k_{off} or k_D, is essential. Furthermore, while immunoglobulin G (IgG) possesses a weak affinity (in our model, α 0.8-0.95) to mucins, immunoglobulin M (IgM) possesses a much stronger affinity (a lower α 0.5), which may be critical in the case of exceptionally low Ab titers (Wessler et al., 2016). Ab therapies will also be heavily dependent on the specific viral infection. Not only will binding affinities vary, but also virus properties such as the number of viral spikes can be vastly different. While SARS-CoV-2 has on the order of 24 spikes, other respiratory viruses such as influenza has 100 s of spikes (Wrigley, 1979). The large number of spikes and consequent ability to bind more Ab more quickly suggests that muco-trapping Ab may be an even more potent therapy against influenza and other viruses with a large number of spikes.

In addition to these protective mechanisms, we are aware that Ab are critical players in a very complex and diverse immune system, and play other roles—such as agglutination (Chen et al., 2015; Xu et al., 2019), initiating the classical pathway for the complement cascade, and as an important part of activation of macrophages to mount an adaptive immune response. Interferons also play an important role in signaling the immune system to enhance its defenses (Le Page et al., 2000; Katze et al., 2002), and a companion submission examines this role in protecting against alveolar pneumonia (Aristotelous et al., 2022).

CRediT authorship contribution statement

Alex Chen: Conceptualization, Data curation, Formal analysis, Funding acquisition, Investigation, Methodology, Software, Validation, Visualization, Writing – original draft, Writing – review & editing. **Timothy Wessler:** Conceptualization, Methodology, Software, Visualization, Writing – original draft. **M. Gregory Forest:** Conceptualization, Formal analysis, Funding acquisition, Methodology, Writing – original draft, Writing – review & editing.

Declaration of Competing Interest

The authors declare that they have no known competing financial interests or personal relationships that could have appeared to influence the work reported in this paper.

Acknowledgments

This research was supported in part by: RSCA grant from CSU Dominguez Hills, NSF-DMS-2028758 (AC), NSF-DMS-1929298 (TW), NSF DMS-1929298, DMS-2028758, NSF DMS-1664645, and NSF CISE-1931516 (MGF) and the North Carolina Policy Collaboratory at the University of North Carolina at Chapel Hill with funding from the North Carolina Coronavirus Relief Fund established and appropriated by the North Carolina General Assembly (MGF). The authors are grateful for discussions with Samuel Lai, Ronit Freeman, Raymond Pickles, and Richard Boucher on SARS-CoV-2, lung geometry, and antibodies. MGF acknowledges valuable communications with multiple members of the IMAG/MSM Working Group. The authors would like to thank the anonymous referees for valuable comments, information, suggestions and references that contributed to the final version of this paper.

References

Aristotelous, A., Chen, A., Forest, M.G. 2022. "A hybrid discrete-continuum model of antibody and interferon immune responses to SARS-CoV-2 infection in the lung alveolar region," *J. Theor. Biol. to appear*.

Beule, A., 2010. Physiology and pathophysiology of respiratory mucosa of the nose and the paranasal sinuses. *GMS Curr. Top. Otorhinolaryngol. - Head Neck Surg.* 9.

Carruthers, J., Xu, J., Finnie, T., Hall, I. 2022. "A within-host model of SARS-CoV-2 infection," *medRxiv*.

Chen, A., McKinley, S., Wang, S., Shi, F., Mucha, P., Forest, M.G., Lai, S., 2014. Transient antibody-mucin interactions produce a dynamic molecular shield against viral invasion. Biophys. J. 106, 2028–2036.

Chen, A., McKinley, S., Shi, F., Wang, S., Mucha, P., Harit, D., Forest, M.G., Lai, S., 2015. Modeling of virion collisions in cervicovaginal mucus reveals limits on agglutination as the protective mechanism of secretory immunoglobulin A. PLoS One 10 (7), e0131351.

Chen, A., Wessler, T., Daftari, K., Hinton, K., Boucher, R., Pickles, R., Freeman, R., Lai, S., Forest, M.G., 2022. Modeling insights into SARS-CoV-2 respiratory tract infections prior to immune protection. Biophys. J. 121 (9), 1619–1631.

Cruz-Teran, C., Tiruthani, K., McSweeney, M., Ma, A., Pickles, R., Lai, S., 2021. Challenges and opportunities for antiviral monoclonal antibodies as COVID-19 therapy. Adv. Drug Deliv. Rev. 169, 100–117.

Despres, H., Mills, M., Shirley, D., Schmidt, M., Huang, M., Jerome, K., Greninger, A., Bruce, E., 2022. Measuring infectious SARS-CoV-2 in clinical samples reveals a higher viral titer:RNA ratio for Delta and Epsilon vs. Alpha variants. *Proc. Natl. Acad. Sci.* 119 (5) e2116518119.

Goyal, A., Reeves, D., Cardozo-Ojeda, E., Schiffer, J., Mayer, B., 2021. Viral load and contact heterogeneity predict SARS-CoV-2 transmission and super-spreading events. *eLife* 10, e63537.

Hessell, A., Rakasz, E., Poignard, P., Hangartner, L., Landucci, G., Forthal, D., Koff, W., Watkins, D., Burton, D., 2009. Broadly neutralizing human anti-HIV antibody 2G12 is effective in protection against mucosal SHIV challenge even at low serum neutralizing titers. PLoS Pathog. 5 (5), e1000433.

Hou, Y., Okuda, K., Edwards, C., Martinez, D., Asakura, T., Dinnon III, K., Kato, T., Lee, R., Yount, B., Mascenik, T., Chen, G., 2020. SARS-CoV-2 reverse genetics reveals a variable infection gradient in the respiratory tract. Cell 182 (2), 429–446.

Hui, K., Ho, J., Cheung, M., Ng, K., Ching, R., Lai, K., Kam, T., Gu, H., Sit, K., Hsin, M., Au, T., 2022. SARS-CoV-2 Omicron variant replication in human bronchus and lung ex vivo. Nature 603 (7902), 715–720.

Jensen, M., Wang, Y.-Y., Lai, S., Forest, M.G., McKinley, S., 2019. Antibody-mediated immobilization of virions in mucus. Bull. Math. Biol. 81 (10), 4069–4099.

Johnson, G., Morawska, L., 2009. The mechanism of breath aerosol formation. J. Aerosol Med. Pulmonary Drug Delivery 22 (3), 229–237.

Jøssang, T., Feder, J., Rosenqvist, E., 1988. Photon correlation spectroscopy of human IgG. J. Protein Chem. 7 (2), 165–171.

Katze, M., He, Y., Gale, M., 2002. Viruses and interferon: a fight for supremacy. Nat. Rev. Immunol. 2 (9), 675–687.

Ke, Z., Oton, J., Qu, K., Cortese, M., Zila, V., McKeane, L., Nakane, T., Zivanov, J., Neufeldt, C., Cerikan, B., Lu, J., 2020. Structures and distributions of SARS-CoV-2 spike proteins on intact virions. Nature 588 (7838), 498–502.

Ke, R., Zitzmann, C., Ho, D., Ribeiro, R., Perelson, A., 2021. In vivo kinetics of SARS-CoV-2 infection and its relationship with a person's infectiousness. *Proc. Natl. Acad. Sci.* 118 (49).

Kissler, S., Fauver, J., Mack, C., Olesen, S., Tai, C., Shiue, K., Kalinich, C., Jednak, S., Ott, I., Vogels, C., Wohlgemuth, J., 2021. Viral dynamics of acute SARS-CoV-2 infection and applications to diagnostic and public health strategies. PLoS Biol. 19 (7), e3001333.

Klasse, P., 2014. Neutralization of virus infectivity by antibodies: old problems in new perspectives. Adv. Biol.

Knowles, M., Boucher, R., 2002. Mucus clearance as a primary innate defense mechanism for mammalian airways. J. Clin. Invest. 109 (5), 571–577.

Kushalnagar, P., Chow, C., Bax, A., 2021. Self-infection with speech aerosol may contribute to COVID-19 severity. J. Intern. Med.

Lai, S., Hida, K., Shukair, S., Wang, Y., Figueiredo, A., Cone, R., Hope, T., Hanes, J., 2009. Human immunodeficiency virus type 1 is trapped by acidic but not by neutralized human cervicovaginal mucus. J. Virol. 83 (21), 11196–11200.

Lai, S., McSweeney, M., Pickles, R., 2021. Learning from past failures: challenges with monoclonal antibody therapies for COVID-19. J. Control. Release 329, 87–95.

Laue, M., Kauter, A., Hoffmann, T., Möller, L., Michel, J., Nitsche, A., 2021. Morphometry of SARS-CoV and SARS-CoV-2 particles in ultrathin plastic sections of infected Vero cell cultures. Sci. Rep. 11 (1), 1–11.

Le Page, C., Genin, P., Baines, M., Hiscott, J., 2000. Interferon activation and innate immunity. Rev. Immunogenetics 2 (3), 374–386.

Li, W., Chen, C., Drelich, A., Martinez, D., Gralinski, L., Sun, Z., Schäfer, A., Kulkarni, S., Liu, X., Leist, S., Zhelev, D., 2020. Rapid identification of a human antibody with

high prophylactic and therapeutic efficacy in three animal models of SARS-CoV-2 infection. *Proc. Natl. Acad. Sci.* 117 (47), 29832–29838.
Matsui, H., Randell, S., Peretti, S., Davis, C.W., Boucher, R., 1998. Coordinated clearance of periciliary liquid and mucus from airway surfaces. J. Clin. Invest. 102 (6), 1125–1131.
McKinley, S., Chen, A., Shi, F., Wang, S., Mucha, P., Forest, M.G., Lai, S., 2014. Modeling neutralization kinetics of HIV by broadly neutralizing monoclonal antibodies in genital secretions coating the cervicovaginal mucosa. PLoS One 9 (6), e100598.
McSweeney, M., Stewart, I., Richardson, Z., Kang, H., Park, Y., Kim, C., Tiruthani, K., Wolf, W., Schaefer, A., Kumar, P., Aurora, H., 2022. Stable nebulization and muco-trapping properties of Regdanvimab/IN-006 supports its development as a potent, dose-saving inhaled therapy for COVID-19. *Bioeng. Transl. Med.* e10391.
Moench, T., Botta, L., Farrer, B., Lickliter, J., Kang, H., Park, Y., Kim, C., Hoke, M., Brennan, M., McSweeney, M., Richardson, Z., 2022. A randomized, double-blind, Phase 1 study of IN-006, an inhaled antibody treatment for COVID-19. *medRxiv*.
Moog, C., Dereuddre-Bosquet, N., Teillaud, J., Biedma, M., Holl, V., Van Ham, G., Heyndrickx, L., Van Dorsselaer, A., Katinger, D., Vcelar, B., Zolla-Pazner, S., 2014. Protective effect of vaginal application of neutralizing and nonneutralizing inhibitory antibodies against vaginal SHIV challenge in macaques. Mucosal Immunol. 7 (1), 46–56.
Morawska, L.J.G.R., Johnson, G., Ristovski, Z., Hargreaves, M., Mengersen, K., Corbett, S., Chao, C., Li, Y., Katoshevski, D., 2009. Size distribution and sites of origin of droplets expelled from the human respiratory tract during expiratory activities. J. Aerosol Sci. 40 (3), 256–269.
Moses, M., Hofmeyr, S., Cannon, J., Andrews, A., Gridley, R., Hinga, M., Leyba, K., Pribisova, A., Surdidijaja, V., Tasnim, H., Forrest, S., 2021. Spatially distributed infection increases viral load in a computational model of SARS-CoV-2 lung infection. PLoS Comput. Biol. 17 (12), e1009735.
Newby, J., Schiller, J., Wessler, T., Forest, M.G., Lai, S., 2017. A blueprint for robust crosslinking of mobile species in biogels with weakly adhesive molecular anchors. Nat. Commun. 8 (1), 1–10.
Newby, J., Seim, I., Lysy, M., Ling, Y., Huckaby, J., Lai, S., Forest, M.G., 2018. Technological strategies to estimate and control diffusive passage times through the mucus barrier in mucosal drug delivery. Adv. Drug Deliv. Rev. 124, 64–81.
Olmsted, S., Padgett, J., Yudin, A., Whaley, K., Moench, T., Cone, R., 2001. Diffusion of macromolecules and virus-like particles in human cervical mucus. Biophys. J. 81 (4), 1930–1937.
Pearson, J., Wessler, T., Chen, A., Boucher, R., Pickles, R., Freeman, R., Lai, S., Forest, M. G., 2022. Modeling predicts mechanisms altered by mutations of the SARS-CoV-2 delta and omicron variants. bioRxiv. https://doi.org/10.1101/2019.12.11.123456.
Quirouette, C., Younis, N., Reddy, M., Beauchemin, C., 2020. A mathematical model describing the localization and spread of influenza A virus infection within the human respiratory tract. PLoS Comput. Biol. 16 (4), e1007705.
Rerks-Ngarm, S., Pitisuttithum, P., Nitayaphan, S., Kaewkungwal, J., Chiu, J., Paris, R., Premsri, N., Namwat, C., de Souza, M., Adams, E., Benenson, M., 2009. Vaccination with ALVAC and AIDSVAX to prevent HIV-1 infection in Thailand. N. Engl. J. Med. 361 (23), 2209–2220.
Rygg, A., Longest, P., 2016. Absorption and clearance of pharmaceutical aerosols in the human nose: development of a CFD model. J. Aerosol Med. Pulmonary Drug Delivery 29 (5), 416–431.
Saltzman, W., Radomsky, M., Whaley, K., Cone, R., 1994. Antibody diffusion in human cervical mucus. Biophys. J. 66 (2), 508–515.
Schaefer, A., Lai, S., 2022. The biophysical principles underpinning muco-trapping functions of antibodies. Hum. Vaccines Immunotherapeutics 18 (2), 1939605.
Schroeder, H., Newby, J., Schaefer, A., Subramani, B., Tubbs, A., Forest, M.G., Miao, E., Lai, S., 2020. LPS-binding IgG arrests actively motile Salmonella Typhimurium in gastrointestinal mucus. Mucosal Immunol. 13 (5), 814–823.
Sender, R., Bar-On, Y., Gleizer, S., Bernshtein, B., Flamholz, A., Phillips, R., Milo, R., 2021. The total number and mass of SARS-CoV-2 virions. *Proc. Natl. Acad. Sci.* 118 (25) e2024815118.
Wang, Y., Kannan, A., Nunn, K., Murphy, M., Subramani, D., Moench, T., Cone, R., Lai, S., 2014. IgG in cervicovaginal mucus traps HSV and prevents vaginal herpes infections. Mucosal Immunol. 7 (5), 1036–1044.
Wang, Y., Harit, D., Subramani, D., Arora, H., Kumar, P., Lai, S., 2017. Influenza-binding antibodies immobilise influenza viruses in fresh human airway mucus. Eur. Respir. J. 49 (1).
Wessler, T., Chen, A., McKinley, S., Cone, R., Forest, M.G., Lai, S., 2016. Using computational modeling to optimize the design of antibodies that trap viruses in mucus. ACS Infect. Dis. 2 (1), 82–92.
Wolfel, R., Corman, V., Guggemos, W., 2020. Virological assessment of hospitalized patients with COVID-2019. Nature 581 (7809), 465–469.
Wrigley, N., 1979. Electron microscopy of influenza virus. Br. Med. Bull. 35 (1), 35–38.
Xu, F., Newby, J., Wessler, T., Chen, A., Schiller, J., Schroder, H., Forest, M.G., Lai, S., 2019. Modeling barrier properties of intestinal mucus reinforced with IgG and secretory IgA against motile bacteria. ACS Infect. Dis. 5 (9), 1570–1580.
Yang, F., Pahlavan, A., Mendez, S., Abkarian, M., Stone, H., 2020. Towards improved social distancing guidelines: space and time dependence of virus transmission from speech-driven aerosol transport between two individuals. Phys. Rev. Fluids 5 (12), 122501.
Yang, B., Schaefer, A., Wang, Y., McCallen, J., Lee, P., Newby, J., Arora, H., Kumar, P., Zeitlin, L., Whaley, K., McKinley, S., 2018. ZMapp reinforces the airway mucosal barrier against Ebola virus. J. Infect. Dis. 218 (6).